Dynamical Systems: An International Journal
Vol. 00, No. 00, June 2005, 1–25

A codimension-two resonant bifurcation from a heteroclinic cycle with complex eigenvalues

Claire M. Postlethwaite[1] and Jonathan H. P. Dawes[1]

(November 1, 2005)

Robust heteroclinic cycles between equilibria lose stability either through local bifurcations of their equilibria or through global bifurcations. This paper considers a global loss of stability termed a 'resonant' bifurcation. This bifurcation is usually associated with the birth or death of a nearby periodic orbit, and generically occurs in either a supercritical or subcritical manner. For a specific robust heteroclinic cycle between equilibria with complex eigenvalues we examine the codimension-two point that separates the supercritical and subcritical. We investigate the bifurcation structure and show the existence of further bifurcations of periodic orbits.

1 Introduction

Dynamical systems with symmetry are widely recognised to naturally have properties that would be very special in the absence of such symmetry. This change in the notion of generic behaviour for symmetric systems has motivated a great deal of work, particularly in developing a symmetric setting for bifurcation theory for ordinary differential equations [1, 2]. At the same time it has been recognised that properties imparted by symmetry can also arise in other ways, for example in mathematical ecology or game theory [3]. An important example of such a property is the existence of flow-invariant subspaces. In the symmetric setting these subspaces arise due to the equivariance of the dynamics with respect to some symmetry group Γ: the symmetries of a solution cannot change as it evolves in time. In the ecological setting the flow-invariance is a biologically reasonable restriction: once a population is extinct it is not possible to generate new individuals.

A heteroclinic cycle is a topological circle of connecting orbits between saddle-type equilibria. In generic (non-symmetric) systems such cycles are of high codimension. However, one consequence of the existence of invariant subspaces is that connecting orbits can be contained within these subspaces. The

[1] DAMTP, Centre for Mathematical Sciences, University of Cambridge, Wilberforce Road, Cambridge CB3 0WA

connecting orbits then persist in the presence of perturbations of the vector field, as long as those perturbations preserve the invariance of the subspaces. Such connecting orbits are termed 'robust'. A heteroclinic cycle made up of equilibria and robust connecting orbits is termed a 'robust heteroclinic cycle'. In the case that all equilibria lie on the same group orbit, the cycle is often termed a 'robust homoclinic cycle'. Robust cycles are natural objects of study in the setting of symmetric dynamics, mathematical ecology or game theory and have occurred in a wide variety of models for intermittent dynamics in physical and biological systems. The review by Krupa [4] discusses many examples and provides further background.

A prototypical example of a robust heteroclinic cycle in $\mathbb{R}^3$ is that discussed by Guckenheimer and Holmes [5]. It arises from an analysis of Busse and Heikes [6] of the Küppers–Lortz instability of thermal convection rolls in a rotating fluid layer, and was also independently proposed as a model of three competing species [7].

For the types of cycles we study in this paper, dynamical stability results depend only on certain genericity assumptions and on eigenvalues of the flow linearised about the equilibria. Krupa and Melbourne [8] give sufficient conditions for the asymptotic stability of a class of robust cycles. An important result is that the so-called 'radial' eigenvalues do not play a part in stability conditions. In $\mathbb{R}^4$, Chossat et al. [9] propose a classification of homoclinic cycles into three types (denoted A, B and C) which are distinguished by the existence, or lack, of a fixed-point subspace that contains the cycle, and the action of the symmetry group on this subspace. A later paper by Krupa and Melbourne [10] extends this classification and gives improved conditions for asymptotic stability of some cycles. In higher dimensions a complete derivation of conditions for stability is lacking, but some recent progress has been made [11].

For homoclinic cycles in $\mathbb{R}^n$, $n \geq 4$, there are (at least) two different ways for robust cycles to lose stability: these are termed 'transverse' and 'resonant' bifurcations. Transverse bifurcations occur when one of the transverse eigenvalues at an equilibrium passes through zero; the equilibrium undergoes a local bifurcation. Chossat et al. [9] prove that for homoclinic cycles in $\mathbb{R}^4$ a transverse bifurcation is accompanied by the birth of either a periodic orbit or a new heteroclinic cycle. In higher dimensions, and for more complicated (heteroclinic) cycles, little is known in general.

At a resonant bifurcation the signs of the eigenvalues are unchanged; the eigenvalues satisfy an algebraic condition that determines a global change in the stability properties of the cycle. Resonant bifurcations were first studied in the non-symmetric case by Chow et al. [12] in the context of a bifurcation from a homoclinic orbit. They found that the nature of the bifurcation depends crucially on the global dynamics, specifically, whether or not the stable manifold

of the homoclinic orbit is orientable. There are many studies of higher codimension bifurcations of homoclinic orbits, for instance the codimension-three study of a resonant homoclinic bifurcation by Homburg and Krauskopf [13]. In this paper we study a codimension-two bifurcation from a robust heteroclinic cycle. Our example seems to be the simplest natural example exhibiting this codimension-two bifurcation in a non-degenerate way in a vector field truncated at cubic order.

Except in degenerate cases, the change of stability of a heteroclinic cycle at a resonant bifurcation is intuitively expected to be accompanied by the birth or death of a nearby (long period) periodic orbit. This can occur in both a subcritical and a supercritical manner (see Hofbauer and Sigmund [3]). A notable exception is the standard Guckenheimer–Holmes case using only the third-order Taylor series truncation of the vector field. In this case the dynamics at the point of resonance is degenerate: an equilibrium away from the cycle undergoes a degenerate Hopf bifurcation at the resonant bifurcation point and the system is Hamiltonian. It is expected that the addition of 5th-order terms consistent with the symmetries would break this degeneracy, and periodic orbits would be seen after the resonant bifurcation. However, a detailed study of the effect of the different possible 5th-order terms has not yet been carried out.

In this paper, we consider a robust cycle, X, between symmetry-related equilibria in $\mathbb{R}^6$ (the cycle is of 'Type C' in the classification given by [10]). Our cycle is similar in structure to the example analysed by Field and Swift [14], but has an additional pair of complex conjugate eigenvalues at each equilibrium, in 'radial' directions. The conditions for asymptotic stability are the same, as the radial eigenvalues do not affect the asymptotic stability of robust heteroclinic cycles (Krupa and Melbourne [8]). The change of stability of the heteroclinic cycle creates an exponentially flat branch of periodic orbits, and the exact nature of the global flow determines whether the bifurcation occurs sub- or supercritically. This is also the case for the homoclinic bifurcation in [12] and the transverse bifurcations of heteroclinic cycles in [9].

Our analysis assumes that all equilibria are hyperbolic and that the flow in a neighbourhood of each equilibrium can be linearised. In fact, these assumptions are generic, since the existence of the invariant subspaces near the equilibria mean that there exists a smooth (C^1) linearisation, even if there are resonances between the eigenvalues (see Hofbauer [15]).

We now describe the main results of this paper.

- The resonant bifurcation of X creates a 'flat' branch of periodic orbits. These periodic orbits undergo a further series of saddle-node bifurcations due to the twisting of the flow on the stable manifold.
- In a two-parameter bifurcation diagram, the curve of saddle-node bifurca-

tions of periodic orbits has a self-similar structure organised around the codimension-two point of the resonant bifurcation.
- At the codimension-two point, there exists an infinity of periodic orbits. Near the codimension-two point there exists a stable periodic orbit arbitrarily close to a stable homoclinic cycle.

The paper is organised as follows. In section 2 we review briefly the definition and structure of robust heteroclinic cycles, and describe the system containing the particular cycle we study. Section 3 describes the construction of Poincaré maps, and in section 4 we investigate fixed points of these maps - these correspond to periodic orbits in the original vector field. We also show results of numerical investigations. In section 5 we analyse the codimension-two point about which the bifurcations of the periodic orbits are organised, and compare the analytical and numerical results. Section 6 concludes.

2 Description of system and symmetries

2.1 *Definitions*

We first recall the notion of a robust heteroclinic cycle and give some definitions. For more details see [8] and [10].

Let $\Gamma \subset \mathbf{O}(n)$ be a finite group acting linearly on $\mathbb{R}^n$, and $f : \mathbb{R}^n \to \mathbb{R}^n$ a Γ-equivariant vector field. We say there is a heteroclinic connection γ_j between two equilibria ξ_j and ξ_{j+1} of f if $\gamma_j(t) \in \mathbb{R}^n$ is a solution of $\dot{x} = f(x)$ which is backward asymptotic to ξ_j and forward asymptotic to ξ_{j+1}. A heteroclinic cycle is an invariant set $X \subset \mathbb{R}^n$ consisting of the union of a set of equilibria $\{\xi_1, ..., \xi_m\}$ of f and orbits $\{\gamma_1, ..., \gamma_m\}$, where γ_j is a heteroclinic connection between ξ_j and ξ_{j+1}; and $\xi_{m+1} \equiv \xi_1$.

For $\Sigma \subset \Gamma$ a subgroup of Γ, we define the fixed-point subspace

$$\text{Fix } \Sigma = \{x \in \mathbb{R}^n : \sigma x = x \ \forall \sigma \in \Sigma\}.$$

Definition 2.1 X is a *robust heteroclinic cycle* if for each j, $1 \leq j \leq m$ there exists a fixed point subspace, $P_j = \text{Fix } \Sigma_j$ where $\Sigma_j \subset \Gamma$ and

(i) ξ_j is a saddle and ξ_{j+1} is a sink in P_j
(ii) there is a heteroclinic connection from ξ_j to ξ_{j+1} in P_j

(indices are to be taken mod m).

It is important to classify the eigenvalues of the linearisation of f at each equilibrium into four classes: radial, contracting, expanding and transverse. Table 1 defines each of these classes according to the subspaces in which the eigenspaces lie. $P \ominus L$ denotes the orthogonal complement in P of the subspace

Table 1. Classification of eigenvalues of $Df(\xi_j)$ at an equilibrium point ξ_j on the cycle. $P \ominus L$ denotes the orthogonal complement of the subspace L within the subspace P.

Eigenvalue class	Subspace
Radial (r)	$L_j \equiv P_{j-1} \cap P_j$
Contracting (c)	$V_j(c) = P_{j-1} \ominus L_j$
Expanding (e)	$V_j(e) = P_j \ominus L_j$
Transverse (t)	$V_j(t) = (P_{j-1} + P_j)^{\perp}$

L. The notation P and L is purposefully suggestive of planes and lines, but it is important to note that $\dim(L)$ may be greater than one. We set $c, r, t < 0$ and $e > 0$ and restrict our attention to the case where $V_j(e)$ is one dimensional; hence the unstable manifold $W^u(\xi_j)$ is one dimensional. This prevents the formation of heteroclinic networks [16].

2.2 *Example system*

In this section we describe the specific heteroclinic cycle studied in the remainder of this paper. We consider a continuous time Γ-equivariant dynamical system (defined by a set of ODEs) with phase space $\mathbb{R}^6$. We denote points $x \in \mathbb{R}^6$ by $x = (x_1, x_2, x_3, x_4, x_5, x_6)$. Let

$$\Gamma = \mathbb{Z}_6 \ltimes \Delta_6 \tag{1}$$

where $\Delta_6 = (\mathbb{Z}_2)^6$ is generated by reflections $\kappa_1, \ldots, \kappa_6$ in each coordinate hyperplane:

$$\kappa_1(x) = (-x_1, x_2, x_3, x_4, x_5, x_6)$$

and similarly for $\kappa_2, \ldots, \kappa_6$. These reflections guarantee that any coordinate hyperplane is an invariant subspace. $\mathbb{Z}_6$ is generated by a permutation of the coordinate axes:

$$\rho(x_1, x_2, x_3, x_4, x_5, x_6) = (x_6, x_1, x_2, x_3, x_4, x_5). \tag{2}$$

Clearly this action of Γ on $\mathbb{R}^6$ is absolutely irreducible. It is clearly also sufficient to consider the dynamics restricted to the domain

$$\mathbb{R}^6_+ = \{(x_1, \ldots, x_6) \in \mathbb{R}^6 | x_1, \ldots, x_6 \geq 0\}.$$

We consider ODEs of the form

$$\dot{x} = f(x, \mu, \nu) \equiv \lambda(\mu, \nu)x + Q(x, \mu, \nu) \tag{3}$$

where f is Γ-equivariant: $\gamma f(x,\mu,\nu) = f(\gamma x,\mu,\nu)$ and μ and ν are bifurcation parameters. We set $\lambda > 0$ and let $Q(x,\mu,\nu)$ be a third-order polynomial in x satisfying

$$Q(x)\cdot x < 0 \tag{4}$$

where $x\cdot y$ is the usual inner product on $\mathbb{R}^n$. By the invariant sphere theorem of Field [17] there is an attracting invariant topological 5-sphere $S^5 \in \mathbb{R}^6\setminus\{0\}$ which we denote S. It follows that the intersection $S\cap\mathbb{R}^6_+ = S^+$ is also flow invariant.

Specifically we consider the ODEs

$$\begin{aligned}
\dot{x}_1 &= x_1(1 - X^2 - c_1x_2^2 + e_2x_3^2 - tx_4^2 - c_2x_5^2 + e_1x_6^2)\\
\dot{x}_2 &= x_2(1 - X^2 + e_1x_1^2 - c_1x_3^2 + e_2x_4^2 - tx_5^2 - c_2x_6^2)\\
\dot{x}_3 &= x_3(1 - X^2 - c_2x_1^2 + e_1x_2^2 - c_1x_4^2 + e_2x_5^2 - tx_6^2)\\
\dot{x}_4 &= x_4(1 - X^2 - tx_1^2 - c_2x_2^2 + e_1x_3^2 - c_1x_5^2 + e_2x_6^2)\\
\dot{x}_5 &= x_5(1 - X^2 + e_2x_1^2 - tx_2^2 - c_2x_3^2 + e_1x_4^2 - c_1x_6^2)\\
\dot{x}_6 &= x_6(1 - X^2 - c_1x_1^2 + e_2x_2^2 - tx_3^2 - c_2x_4^2 + e_1x_5^2)
\end{aligned} \tag{5}$$

where $X^2 = \sum_{j=1}^6 x_j^2$, and c_i, e_i, and t are strictly positive parameters. By rescaling time and the coordinates x_i we set the coefficient of the linear terms (λ in (3)) equal to unity, and the coefficient of the x_j^3 term in the x_j equation equal to -1; it follows from (4) that it is negative.

Equations (5) are clearly Γ-equivariant as required. We focus on the equilibrium ξ_1 which is the equilibrium with three non-zero components in the subspace $\{x_4 = x_5 = x_6 = 0\}$; there are five other symmetry-related equilibria, which we denote $\xi_2,\ldots,\xi_6$. To show the existence of a heteroclinic connection from ξ_1 to ξ_2 we consider the four-dimensional invariant subspace $P_1 = \{x_5 = x_6 = 0\} = \mathrm{Fix}(\mathbb{Z}_2^{\kappa_5}\times\mathbb{Z}_2^{\kappa_6})$ in which it must lie. It can be verified that if an equilibrium with four non-zero components exists, for (5), it must be unstable. For an open region of parameter space the flow restricted to P_1, ξ_2 is the only sink and the connection is robust. Applying the definitions in table 1 we deduce that $\dim V_1(c) = \dim V_1(e) = \dim V_1(t) = 1$: the expanding eigenvalue at ξ_1 (λ_e) is in the x_4 direction, the contracting eigenvalue ($-\lambda_c$) is in the x_6 direction and the transverse eigenvalue ($-\lambda_t$) is in the x_5 direction. In contrast, $\dim L_1 = 3$ and we label the radial eigenvalues $-\lambda_r$ and $-\lambda_R \pm \mathrm{i}\lambda_I$. Appendix A contains expressions for these eigenvalues in terms of c_i, e_i and t. A finite number of conditions (hence holding in an open region of parameter space that intersects the region where the robust connections exist)

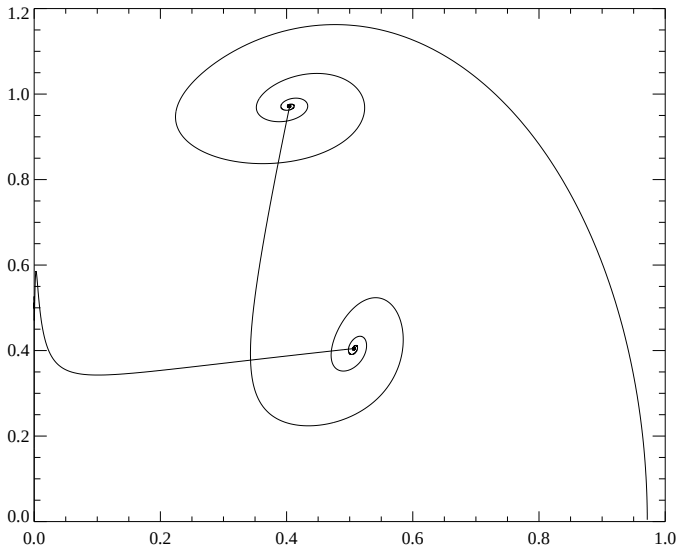

Figure 1. A trajectory approaching a heteroclinic cycle from a numerical simulation of equations (5), projected onto the x_1-x_2 plane. Parameters are $c_1 = 0.65$, $c_2 = 1.0$, $e_1 = 3.8$, $e_2 = 0.5$, $t = 1.1$.

ensure that the eigenvalues have the correct signs and that the conditions for invariant sphere theorem to apply are satisfied. These conditions are not given explicitly, but we have verified that they hold for the region of parameter space we investigate numerically.

We remark that the eigenspaces satisfy the conditions for a type C cycle given in Krupa and Melbourne [10], that is, there exist subspaces Q_j, R_j, $1 \leq j \leq 6$ (j taken mod 6), such that

$$Q_j = P_j \oplus V_j(c) = P_j \oplus V_{j+1}(t) \tag{6}$$

$$R_j = P_j \oplus V_j(t) = P_j \oplus V_{j+1}(e) \tag{7}$$

Figure 1 shows a trajectory very close to a heteroclinic cycle from a numerical integration of (5). Notice the spiralling approach to, and monotonic departure from, each equilibrium. For the numerics, we introduce new variables $X_j = \log(x_j)$, and integrate the transformed equations instead of integrating equations (5) directly. These new equations are valid in the interior of $\mathbb{R}^6_+$ which is invariant, along with its boundaries. In particular, any periodic orbits that bifurcate from the cycle will all be contained in the interior of $\mathbb{R}^6_+$. Our change of variables significantly reduces numerical error. The numerical integrations of the new equations were performed using a standard RK4 integrator with a timestep $dt = 0.01$.

3 Construction of Poincaré maps

We construct Poincaré maps to approximate the flow $\dot{x} = f(x, \mu, \nu)$ near the heteroclinic cycle. This enables us to study the dynamics of trajectories close to the heteroclinic cycle, to calculate the stability of the cycle, and to determine the location and stability of nearby periodic orbits. We define coordinates and Poincaré sections about the equilibria, and write down local and global maps approximating the flow in the usual way.

We chose local Cartesian coordinates about ξ_1: $(x_X, x_Y, x_c, x_t, x_e)$ spanning the spaces $L_1 \cap S$ (of dimension 2), $V_1(c)$, $V_1(t)$ and $V_1(e)$ respectively. The linearised flow about ξ_1 is:

$$\begin{aligned}
\dot{x}_X &= -\lambda_R x_X - \lambda_I x_Y \\
\dot{x}_Y &= \lambda_I x_X - \lambda_R x_Y \\
\dot{x}_c &= -\lambda_c x_c \\
\dot{x}_t &= -\lambda_t x_t \\
\dot{x}_e &= \lambda_e x_e
\end{aligned}$$

It is useful to define polar coordinates (r, θ) by $x_X = r\cos\theta$ and $x_Y = r\sin\theta$. In the following we will often interchange pairs (x_X, x_Y) with (r, θ); this will be obvious from the context. We define two Poincaré sections near ξ_1:

$$\begin{aligned}
H^{\text{in}} &= \{(r, \theta, x_c, x_t, x_e) : r^2 + x_c^2 = h^2, 0 < \theta \leq 2\pi, 0 \leq x_t, x_e \leq h\} \\
H^{\text{out}} &= \{(r, \theta, x_c, x_t, x_e) : x_e = h, 0 < \theta \leq 2\pi, 0 \leq r, x_t, x_c \leq h\}
\end{aligned}$$

where $0 < h \ll 1$ is a constant. When h is small enough we expect that the heteroclinic connection intersects H^{in} and H^{out} transversely. It is then simple to write down a local map $\phi : H^{\text{in}} \to H^{\text{out}}$ integrating the linearised flow:

$$\phi \begin{pmatrix} r \\ \theta \\ x_c \\ x_t \\ x_e \end{pmatrix} = \begin{pmatrix} r\left(\frac{x_e}{h}\right)^{\frac{\lambda_R}{\lambda_e}} \\ \theta - \frac{\lambda_I}{\lambda_e}\ln\left(\frac{x_e}{h}\right) \\ x_c\left(\frac{x_e}{h}\right)^{\frac{\lambda_c}{\lambda_e}} \\ x_t\left(\frac{x_e}{h}\right)^{\frac{\lambda_t}{\lambda_e}} \\ h \end{pmatrix}$$

The time of flight of the trajectory from H^{in} to H^{out} is given in this linear

approximation by

$$T = -\frac{1}{\lambda_e} \log\left(\frac{x_e}{h}\right). \tag{8}$$

Since $\xi_2 = \rho\xi_1$, the Poincaré sections near ξ_2 can be defined by ρH^{in} and ρH^{out}. The second element of the construction is a global map $\varphi : H^{\text{out}} \to \rho H^{\text{in}}$ to approximate the part of the flow near the heteroclinic connection. Firstly we label the point of intersection of the unstable manifold of ξ_1 (that is, the heteroclinic connection) with ρH^{in} as

$$x = (r^\star, \theta^\star, 0, 0, x^\star) \in \rho H^{\text{in}}; \qquad r^{\star 2} + x^{\star 2} = h^2 \tag{9}$$

and write $X^\star = r^\star \cos\theta^\star$, $Y^\star = r^\star \sin\theta^\star$. In the case $|\lambda_R| < |\lambda_c|$, the trajectory decays onto L_2 (the radial subspace for ξ_2) faster than it spirals in towards $r = 0$. Hence we can always pick h small enough so that $x^\star \ll r^\star$. We will assume from now on that this is the case - the other case is less interesting as there is no twisting of the stable manifold because it approaches the equilibrium tangent to the one-dimensional space $V_2(c)$.

Secondly, the unstable manifold of ξ_1 lies in the subspace $P_1 = V_1(e) + L_1 = \text{Fix}\,(\langle \kappa_c, \kappa_t \rangle)$, (see table 1) and has isotropy $\mathbb{Z}_2^{\kappa_c} \times \mathbb{Z}_2^{\kappa_t}$. The isotypic decomposition of $\mathbb{R}^6$ with respect to $\mathbb{Z}_2^{\kappa_c} \times \mathbb{Z}_2^{\kappa_t}$ is $\mathbb{R}^6 = P_1 \oplus V_1(c) \oplus V_1(t)$. The coordinates x_X, x_Y and x_e span P_1, so the global map $\varphi : H^{\text{out}} \to \rho H^{\text{in}}$, including only constant and linear terms, takes the form

$$\varphi \begin{pmatrix} x_X \\ x_Y \\ x_c \\ x_t \\ h \end{pmatrix} = \begin{pmatrix} X^\star \\ Y^\star \\ 0 \\ 0 \\ x^\star \end{pmatrix} + \begin{pmatrix} a_{11} & a_{12} & 0 & 0 & a_{15} \\ a_{21} & a_{22} & 0 & 0 & a_{25} \\ 0 & 0 & a_{33} & 0 & 0 \\ 0 & 0 & 0 & a_{44} & 0 \\ a_{51} & a_{52} & 0 & 0 & a_{55} \end{pmatrix} \begin{pmatrix} x_X \\ x_Y \\ x_c \\ x_t \\ h \end{pmatrix} \tag{10}$$

where the constants a_{ij} depend on the global flow. We take them to be $O(1)$, and assume certain non-degeneracy conditions that will become clear in due course. Note that the flow invariance of $\mathbb{R}^6_+$ implies $a_{33}, a_{44} > 0$. Composing the local and global maps together with the symmetry ρ^{-1} gives a complete return map $\rho^{-1} \circ \varphi \circ \phi \equiv \psi : H^{\text{in}} \to H^{\text{in}}$:

$$\psi\begin{pmatrix} r \\ \theta \\ x_c \\ x_t \\ x_e \end{pmatrix} = \begin{pmatrix} r^\star + A_r r\left(\frac{x_e}{h}\right)^{\frac{\lambda_R}{\lambda_e}} \cos\left(\frac{\lambda_I}{\lambda_e}\log x_e + \theta + \Phi_r\right) \\ \theta^\star + A_\theta r\left(\frac{x_e}{h}\right)^{\frac{\lambda_R}{\lambda_e}} \cos\left(\frac{\lambda_I}{\lambda_e}\log x_e + \theta + \Phi_\theta\right) \\ x^\star + A_c r\left(\frac{x_e}{h}\right)^{\frac{\lambda_R}{\lambda_e}} \cos\left(\frac{\lambda_I}{\lambda_e}\log x_e + \theta + \Phi_c\right) \\ A_t x_c\left(\frac{x_e}{h}\right)^{\frac{\lambda_c}{\lambda_e}} \\ A_e x_t\left(\frac{x_e}{h}\right)^{\frac{\lambda_t}{\lambda_e}} \end{pmatrix} + \text{h.o.t.}$$

where A_α and Φ_α are functions of the a_{ij} (and hence of the bifurcation parameters μ and ν), and $A_t, A_e > 0$. The dynamics close to the heteroclinic connection are given by initial conditions with r, x_c, x_t and x_e all small. Two components of the return map can be eliminated by approximations that are consistent with our approach. We approximate θ by $\theta^\star$, since the error in the r and x_c components is then of order $r^2(x_e/h)^{2\lambda_R/\lambda_e}$ which is the same order as the terms omitted by taking only the linear terms in (10). We also eliminate the r coordinate: it is determined by the x_c coordinate and the definition of H^{in} (recall $r^2 + x_c^2 = h^2$ on H^{in}). Since $x^\star \ll r^\star$, we may assume $x_c \ll r$ and write $r \approx 1 - x_c^2/2$.

We rescale the remaining coordinates, the constants A_c, A_e, A_t, Φ_c and $x^\star$ for convenience, to obtain the three-dimensional map

$$\psi\begin{pmatrix} x_c \\ x_t \\ x_e \end{pmatrix} = \begin{pmatrix} x^\star + A_c x_e^{\frac{\lambda_R}{\lambda_e}} \cos\left(\frac{\lambda_I}{\lambda_e}\log x_e + \Phi_c\right) \\ A_t x_c x_e^{\frac{\lambda_c}{\lambda_e}} \\ A_e x_t x_e^{\frac{\lambda_t}{\lambda_e}} \end{pmatrix} + O\begin{pmatrix} x_e^{2\frac{\lambda_R}{\lambda_e}} \\ x_c^2 x_e^{2\frac{\lambda_c}{\lambda_e}}, x_c x_t x_e^{\frac{\lambda_c+\lambda_t}{\lambda_e}} \\ x_t^2 x_e^{2\frac{\lambda_t}{\lambda_e}}, x_c x_t x_e^{\frac{\lambda_c+\lambda_t}{\lambda_e}} \end{pmatrix} \tag{11}$$

where $0 < x^\star < 1$, $A_t, A_e > 0$, A_c and Φ_c are $O(1)$. We include here the size of the next order terms; they were omitted for clarity in previous expressions. The stability of the fixed point $(x^\star, 0, 0)$ yields the stability of the heteroclinic cycle in the flow.

For initial conditions very close to the cycle, when $x_t, x_e \ll x^\star$, we can further reduce the dimension of the map by setting $x_c = x^\star$. At leading order we obtain

$$\psi\begin{pmatrix} x_t \\ x_e \end{pmatrix} = \begin{pmatrix} A_t x^\star x_e^{\frac{\lambda_c}{\lambda_e}} \\ A_e x_t x_e^{\frac{\lambda_t}{\lambda_e}} \end{pmatrix} \tag{12}$$

which, as expected, is the map for Type C cycles in $\mathbb{R}^4$ obtained in [14] and [10].

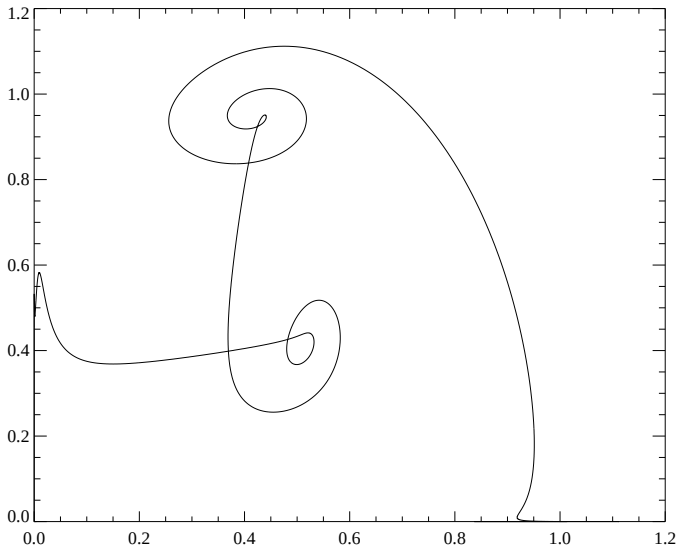

Figure 2. A periodic orbit from a numerical simulation of equations (5), projected onto the x_1-x_2 plane. Parameters are $c_1 = 0.65$, $c_2 = 1.0$, $e_1 = 3.5$, $e_2 = 0.5$, $t = 0.8$.

The condition for the cycle to be asymptotically stable is then easily seen to be $\lambda_c + \lambda_t - \lambda_e > 0$. A resonant bifurcation occurs when this condition is an equality and asymptotic stability is lost.

4 Periodic orbits

We now look at non-trivial fixed points of (11); these correspond to periodic orbits lying close to the heteroclinic cycle. Figure 2 shows an example of such a periodic orbit found in a numerical simulation of (5). Provided the periodic orbits are close enough to the heteroclinic cycle, the higher order terms in (11) can be safely neglected: in the first instance we look for fixed points of (11) using only the leading order terms and taking $x_c = x^\star$ constant: this enables us to determine the stability of the periodic orbits and the subcritical or supercritical nature of the bifurcation. Later we include the full set of leading order terms in (11) and follow periodic orbits further from the global bifurcation. We define bifurcation parameters μ and ν: μ governs the stability of the heteroclinic cycle (so $\mu = 0$ at the resonant bifurcation) while the second bifurcation parameter ν, defined presently, controls whether the bifurcation is subcritical or supercritical.

We define the eigenvalue ratios $\delta = \frac{\lambda_c}{\lambda_e}$ and $\sigma = \frac{\lambda_t}{\lambda_e}$ and will sometimes write $A_t = A_t(\mu, \nu) > 0$ and $A_e = A_e(\mu, \nu) > 0$, to make clear that A_t and A_e are

continuous functions of μ and ν. We assume the non-degeneracy conditions

$$A_t(0,\nu), A_e(0,\nu) \neq 0 \tag{13}$$

We define the bifurcation parameter $\mu = 1 - \sigma - \delta$; the cycle is stable or unstable when $\mu < 0$ or $\mu > 0$. The lowest order terms in the map give

$$\psi \begin{pmatrix} x_c \\ x_t \\ x_e \end{pmatrix} = \begin{pmatrix} x^\star \\ A_t x_c x_e^{1-\sigma-\mu} \\ A_e x_t x_e^\sigma \end{pmatrix} \tag{14}$$

The non-trivial fixed point of this map occurs at

$$\bar{x}_c = x^\star, \qquad \bar{x}_e = B^{\frac{1}{\mu}} \qquad \bar{x}_t = A_t x^\star B^{(1-\sigma-\mu)/\mu}$$

where $B = x^\star A_t A_e$. The coordinates $\bar{x}_e$ and $\bar{x}_t$ will be small and positive (that is, the fixed point corresponds to a periodic orbit in the flow close to the heteroclinic cycle) if either $B < 1$ and $\mu > 0$ or $B > 1$ and $\mu < 0$. It is straightforward to calculate the eigenvalues of the map (14) at the fixed point. They are independent of B, and lie inside the unit circle if $\mu > 0$, so the fixed point corresponds to a stable periodic orbit for the flow. Conversely, when $\mu < 0$ one of the eigenvalues is greater than one and hence the corresponding periodic orbit in the flow is unstable. By the continuous dependence of B and μ on the eigenvalues, if at $\mu = 0$ we have $B < 1$, then $B < 1$ for small enough $\mu > 0$ and the bifurcation is supercritical. Similarly, if at $\mu = 0$ we have $B > 1$, the bifurcation is subcritical. The case $B = 1$ is degenerate, and implicitly defines the codimension-two point. We define the second bifurcation parameter $\nu = B - 1$.

To make a more detailed analysis we include the other terms in the first component of the map (11) as this enables us to locate periodic orbits as we move further from the heteroclinic cycle. Locating fixed points we find

$$\bar{x}_t = A_t \bar{x}_c \bar{x}_e^{\frac{1-\sigma(\mu,\nu)-\mu}{\mu}}, \qquad \bar{x}_e^\mu = A_t A_e \bar{x}_c$$

so

$$\bar{x}_e^\mu = B + A\bar{x}_e^{\frac{\lambda_R}{\lambda_e}} \cos\left(\frac{\lambda_I}{\lambda_e}\log x_e + \Phi_c\right) \tag{15}$$

where $A = A_t A_e A_c$. From (8) the time of flight T, of the trajectory from H^{in} to H^{out}, is given by $\bar{x}_e = \mathrm{e}^{-\lambda_e T}$. The period of the corresponding periodic

orbit is $6T$. Rewriting equation (15) in terms of T yields

$$\mathrm{e}^{-\lambda_e \mu T} = B + A\mathrm{e}^{-\lambda_R T}\cos\left(\lambda_I T + \Phi\right). \tag{16}$$

As $\mu \to 0$ and $T \to \infty$ we deduce the leading order expression

$$\mathrm{e}^{-\lambda_e \mu T} = B \qquad \Rightarrow \qquad \mu \to \frac{-\log B}{\lambda_e T} \tag{17}$$

This reproduces the earlier result that if $B < 1$ then periodic orbits close to the heteroclinic orbit exist in $\mu > 0$, and if $B > 1$ then they exist in $\mu < 0$.

For finite T a series of saddle-node bifurcations occurs, generating more periodic orbits at smaller T. If $\nu \neq 0$ there is a finite number of wiggles, and for T large enough the curve becomes monotonic in the (μ, T) plane. Exactly at $\nu = 0$ there is an infinite sequence of saddle-node bifurcations and so infinitely many periodic orbits exist at $\mu = \nu = 0$.

4.1 *Numerical continuation of saddle-node bifurcations*

For our example ODEs given in section 2.2 we follow the curves of periodic orbits using continuation in the ODE coefficients e_1 and t and the well known continuation package AUTO [18]. In the numerical simulations we introduce a rescaled bifurcation parameter $f = \lambda_e \mu$. Figure 3 illustrates the cases of subcritical and supercritical bifurcations. We obviously cannot calculate $B(\mu, \nu)$ explicitly for our example ODEs, since it depends on the global location of the heteroclinic orbit between the equilibria, but from the preceding analysis expect that $B(0, \nu) > 1$ for 3(a) and $B(0, \nu) < 1$ for 3(b).

The continuation is carried out using the transformed equations described at the end of section 2.2. This decreases the computation time as well as increasing accuracy; the locations of periodic orbits and their bifurcations are unaffected. We are now able to investigate periodic orbits with very high periods, where coordinates routinely become as small as e^{-200}.

The dependence of f $(= \lambda_e \mu)$ on the two coefficients e_1 and t is given explicitly in the Appendix. We remark that B varies implicitly with both coefficients in a way that is difficult to calculate analytically. Shown in figure 4 are the resulting curves, plotted in the (f, t) plane. Notice the nearly self-similar structure of cusps, converging to a point on the line $f = 0$ (where $\nu = 0$). The two plots in figure 3 were taken for t just above and just below this accumulation point.

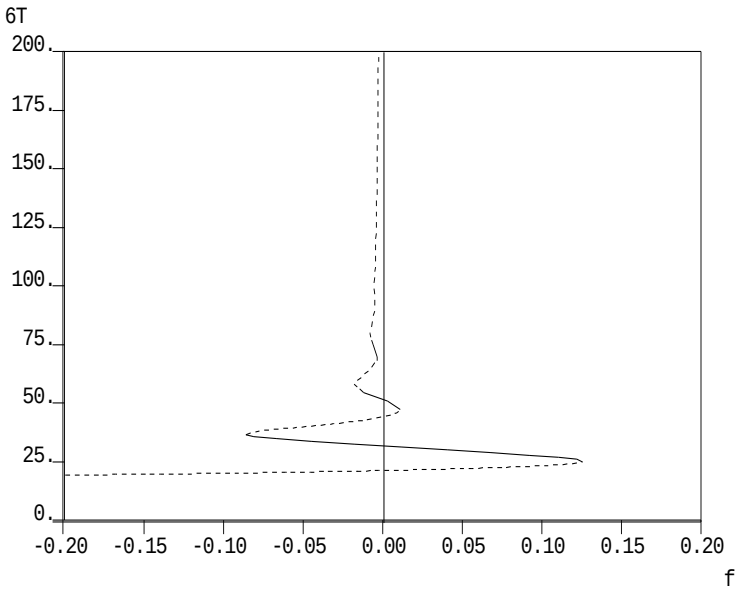

(a) The subcritical case

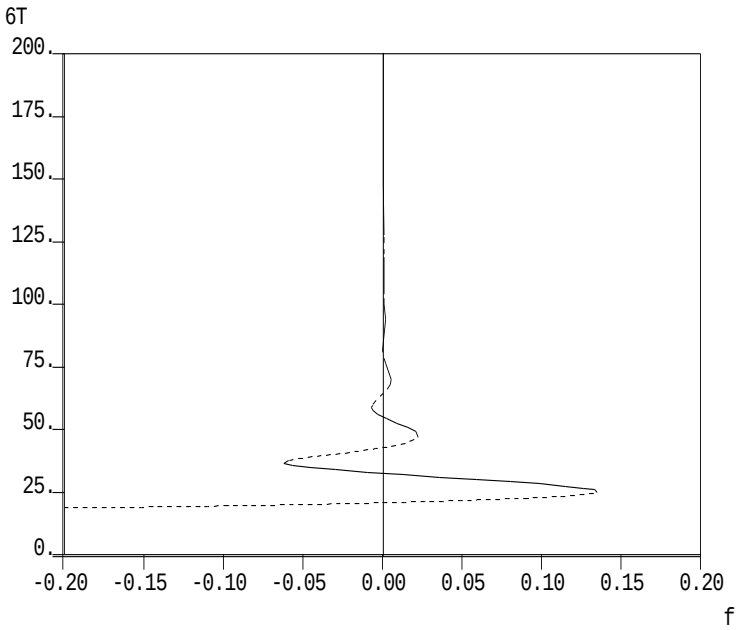

(b) The supercritical case

Figure 3. Curves of periodic orbits in the (f, T) plane. Stable and unstable orbits are shown with solid and dashed lines respectively, illustrating the sequence of saddle-node bifurcations. The heteroclinic cycle is stable in the region $f < 0$. For clarity the vertical line $f = 0$ is given. In (a), the largest period orbits are unstable, and exist in $f < 0$, and the bifurcation is subcritical. In (b), the largest period orbits are stable, and exist in $f > 0$ and the bifurcation is supercritical. For both plots, coefficients are fixed at $c_1 = 0.65$, $c_2 = 1.0$, $e_2 = 0.5$ with continuation carried out in e_1. For figure (a) we take $t = 1.227$, and for (b) $t = 1.03$.

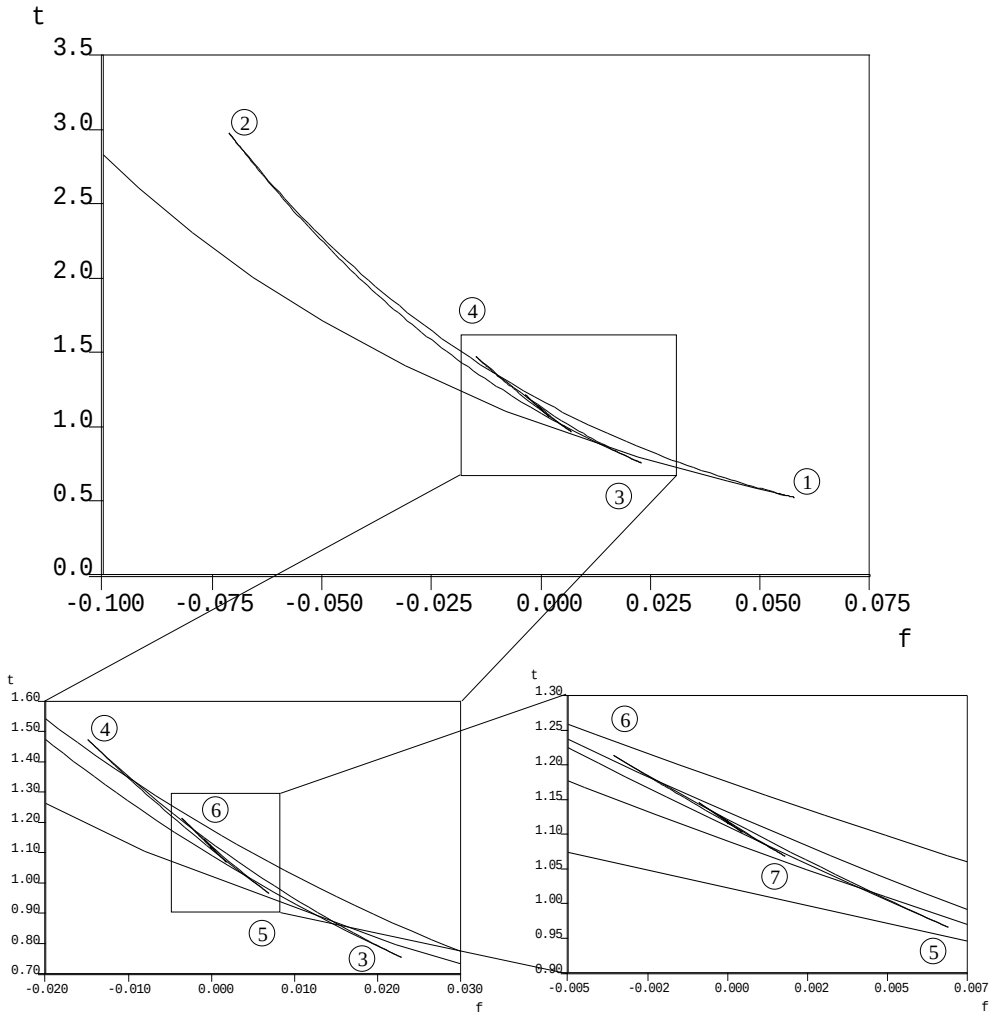

Figure 4. Curves of saddle-node bifurcations in the (f, t) plane, from AUTO output, with coefficient values $c_1 = 0.65$, $c_2 = 1.0$ and $e_2 = 0.5$, with continuation in the remaining two parameters e_1 and t. The accumulation point corresponds to $e_1 = 3.90$ and $t = 1.12$. The lower two figures are successive close ups on the indicated areas. Notice how the sequence of cusps seems to be repeating on smaller and smaller scales. The circled numbers are labels for the cusp points, as referred to in table 2. The periods of the orbits at these points are also shown in table 2. The period of the longest orbit before it is impossible to distinguish changes of sign of f is approximately $6T = 200$.

5 The codimension-two point

At $\mu = \nu = 0$ the resonant heteroclinic bifurcation changes from supercritical to subcritical. The AUTO calculations indicate the structure of the arrangement of the saddle-node bifurcations about this codimension-two point. In this section, we investigate this structure analytically using equation (16). We then

compare our results with the numerical data obtained from AUTO.

We use the parameter $f = \lambda_e \mu$ for convenience, and expand about the codimension-two point $f = \nu = 0$, taking $T \gg 1$. In the expansion we assume that A, Φ, λ_R and λ_I are all order 1, non-zero constants. We rewrite equation (16) as

$$Tf = -\log\left(1 + \nu + A\mathrm{e}^{-\lambda_R T}\cos(\lambda_I T + \Phi)\right) \tag{18}$$

and approximate at leading order in ν and $\mathrm{e}^{-\lambda_R T}$ to find

$$f = \frac{1}{T}\left(-\nu - A\mathrm{e}^{-\lambda_R T}\cos(\lambda_I T + \Phi)\right) + O\left(\frac{\nu^2}{T}, \frac{\mathrm{e}^{-2\lambda_R T}}{T}\right) \tag{19}$$

This first approximation (of the position of the periodic orbits near the codimension-two point) indicates that the relative size of ν and $\mathrm{e}^{-\lambda_R T}$ is important in determining the shape of the curve. If ν dominates, then the curve is monotonic, but if $\mathrm{e}^{-\lambda_R T}$ is of the same order or larger magnitude than ν, then the oscillatory term introduces saddle-node bifurcations.

These saddle-node bifurcations occur when $\frac{df}{dT} = 0$: differentiating (19) we find

$$\frac{df}{dT} = \frac{\nu}{T^2} - R(T)\cos(\lambda_I T + \alpha_1(T) + \Phi) + O\left(\frac{\nu^2}{T^2}, \frac{\mathrm{e}^{-2\lambda_R T}}{T^2}\right), \tag{20}$$

where

$$R(T) = A|\lambda|\mathrm{e}^{-\lambda_R T}\frac{1}{T} + O\left(\frac{\mathrm{e}^{-\lambda_R T}}{T^2}\right) \qquad \text{and} \qquad \tan(\alpha_1(T)) = \frac{-\lambda_I}{\lambda_R + \frac{1}{T}}, \tag{21}$$

and $|\lambda| = (\lambda_R^2 + \lambda_I^2)^{1/2}$. So, when $\frac{df}{dT} = 0$ we find

$$\nu = A|\lambda|T\mathrm{e}^{-\lambda_R T}\cos(\lambda_I T + \alpha_1(T) + \Phi) + O\left(\nu^2, \mathrm{e}^{-\lambda_R T}\right). \tag{22}$$

Figure 5 illustrates the relationship (curve C) between ν and T along the curve of saddle-node bifurcations, for large T.

The first case we consider is the region where we expect saddle-node bifurcations, that is, where $\nu \lesssim \mathrm{e}^{-\lambda_R T}$. The second case is the region where there are no such bifurcations, when $\nu \sim T\mathrm{e}^{-\lambda_R T}$, so $\nu \gg \mathrm{e}^{-\lambda_R T}$.

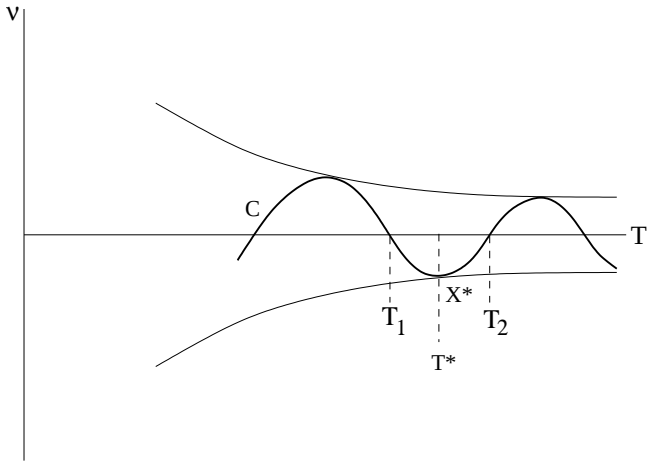

Figure 5. The curve C shows the relationship between ν and T along the curve of saddle-node bifurcations, given by equation (22).

At $\nu = 0$, equation (22) has solutions

$$\cos(\lambda_I T + \alpha_1(T) + \Phi) = O\left(\mathrm{e}^{-\lambda_R T}\right) \ll 1 \tag{23}$$

Suppose (23) is satisfied for some $T = T_1$, sufficiently large, then it will also be satisfied for $T = T_2 \approx T_1 + \pi/\lambda_I$ since to first order $\alpha_1(T)$ is independent of T. So, for $\nu = 0$ and for large enough T, the saddle-node bifurcations occur at a frequency of $\Delta T = \frac{\pi}{\lambda_I}$. These points are indicated in figure 5 (T_1 and T_2). This approximation can be extended into the region of small, nonzero ν. Rearranging (22) gives

$$\begin{aligned}\cos(\lambda_I T + \alpha_1(T) + \Phi) &= -\frac{\nu}{T^2 R(T)} + O\left(\frac{\nu^2 \mathrm{e}^{\lambda_R T}}{T}, \frac{\mathrm{e}^{-\lambda_R T}}{T}\right) \\ &= O\left(\frac{\nu \mathrm{e}^{\lambda_R T}}{T}, \frac{\mathrm{e}^{-\lambda_R T}}{T}\right)\end{aligned} \tag{24}$$

so the same solutions are valid so long as

$$\nu \ll T\mathrm{e}^{-\lambda_R T} \tag{25}$$

which is certainly the case in the region where $\nu \lesssim \mathrm{e}^{-\lambda_R T}$.

We now consider the locations of these saddle-node bifurcations in the f-T plane, and in the f-ν plane. Let the bifurcation at T_1 occur for some $f = f_1$ and the bifurcation at $T_2 > T_1$ for some $f = f_2$. Figure 6(a) shows a sketch of

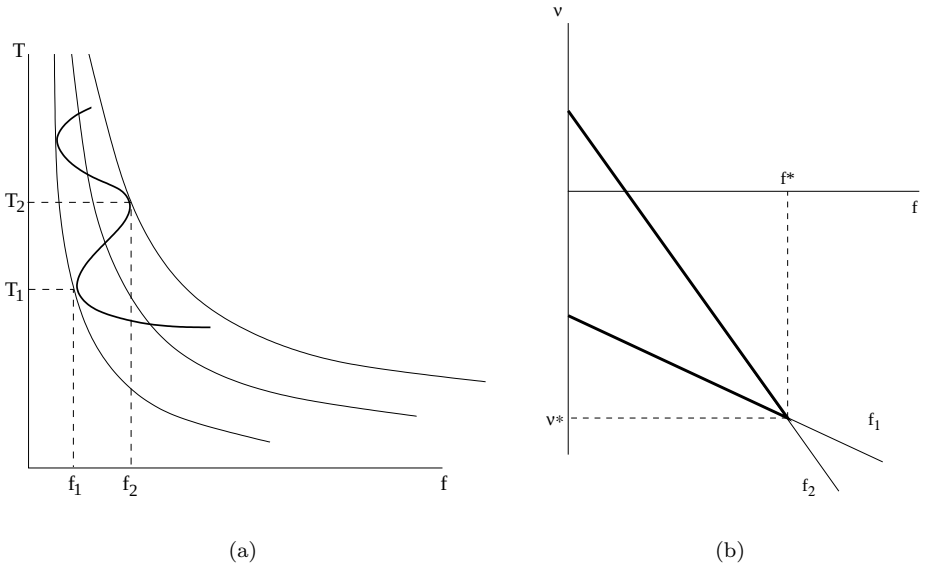

Figure 6. (a) shows a curve of periodic orbits in the f-T plane. f_1 and f_2 are the locations of two saddle-node bifurcations of periodic orbits, and (b) shows how their location changes as ν is varied. The bold line indicates the region where the saddle-node bifurcations exist.

the curve of periodic orbits in the f-T plane, indicating these two bifurcations. Note that the bifurcations only exist when $f_2 > f_1$.

Let $\cos(\lambda_I T_1 + \Phi) = \phi$, then $\cos(\lambda_I T_2 + \Phi) = -\phi$, and from (19) we can write down equations for f_1 and f_2 in terms of ν:

$$f_1 = \frac{-\nu - c_1}{c_2} \qquad f_2 = \frac{-\nu + \mathrm{e}^{-\pi\frac{\lambda_R}{\lambda_I}} c_1}{c_2 + \frac{\pi}{\lambda_I}} \tag{26}$$

where $c_1 = A\phi \mathrm{e}^{-\lambda_R T_1} \ll 1$ and $c_2 = T_1 \gg 1$.

For $\nu \ll T\mathrm{e}^{-\lambda_R T}$, T is independent of f and ν along each curve, and so the curves f_1 and f_2 are straight lines in the f-ν plane, as shown in figure 6(b). We have, in this sketch, extended the lines out of the range of ν for which the approximations are valid, but will come back later and correct this. The main point to take away from this sketch is that when the two curves f_1 and f_2 cross, the two saddle-node bifurcations disappear and the curve of periodic orbits in the f-T plane becomes monotonic in the region $T_1 \le T \le T_2$. The point where they cross corresponds to the point $X^\star$ in figure 5, that is, where ν changes direction for increasing T. The bold line in figure 6(b) is where $f_2 > f_1$, that is, the line of saddle-node bifurcations.

The curves f_1 and f_2 can extend into $f < 0$, where the bifurcation at f_2

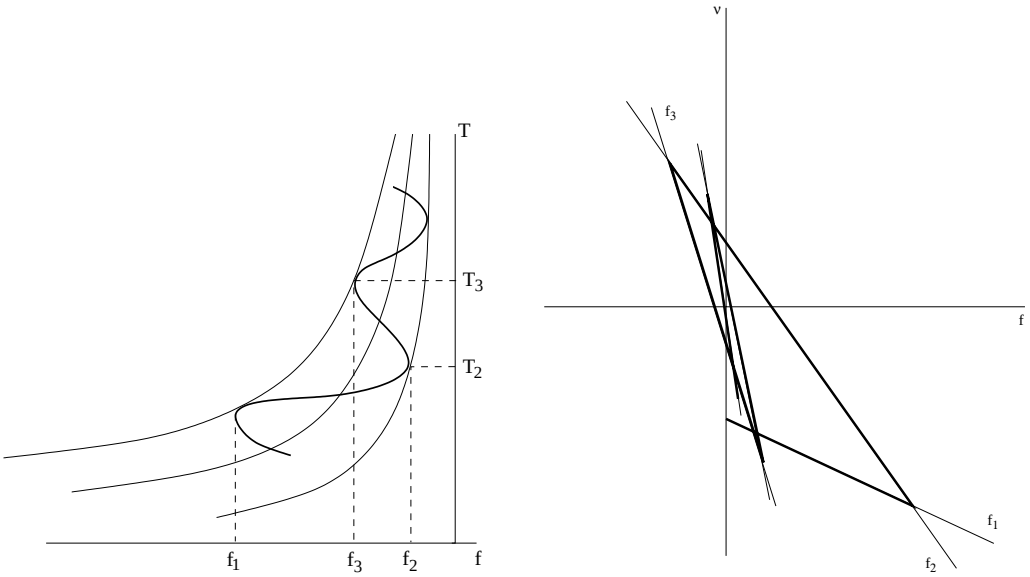

Figure 7. (a) f_2 and f_3 are two saddle-node bifurcations of periodic orbits for $f < 0$. (b) is a continuation of figure 6(b) showing in bold the location of saddle-node bifurcations in the f-ν plane.

collides with a saddle-node bifurcation with larger period, shown as f_3 in figure 7(a). The equation for the location of f_3 is

$$f_3 = \frac{-\nu - \mathrm{e}^{-2\pi\frac{\lambda_R}{\lambda_I}} c_1}{c_2 + \frac{2\pi}{\lambda_I}} \tag{27}$$

and the saddle-node bifurcations at f_2 and f_3 exist if $f_2 > f_3$. Following f_3 back into $f > 0$ and continuing in this manner we find a curve of saddle-node bifurcations of increasing T which spirals in towards $f = \nu = 0$. This is shown schematically in figure 7(b). This figure has obvious structural similarities with figure 4; recall that we do not know the direction of ν in figure 4, so the orientation of the curves is different. Compare this also with figure 5, which shows ν oscillating towards zero as T increases along the curve of saddle-node bifurcations.

We now consider the second region, where $\nu \gg \mathrm{e}^{-\lambda_R T}$. This is the outer region of the sketch in figure 7(b), where the curves f_i cross and the saddle-node bifurcations annihilate each other. We use figure 5 and equation (22) to gain more insight into the shape of the curves f_i in this region: they are no longer well approximated by straight lines. We label the point where the

curves f_1 and f_2 cross as $X^\star = (f^\star, \nu^\star)$ (see figure 6(b)), and let the period of the periodic orbit at this point be $6T^\star$ (also labelled on figure 5).

The portion of curve C in figure 5 from T_1 to $T^\star$ corresponds to the curve f_1 from $\nu = 0$ to the point $X^\star$. Equation (26) still holds outside of the region $\nu \ll T\mathrm{e}^{-\lambda_R T}$, but now c_1 and c_2 are not constants, but complicated functions of ν obtained by inverting equation (22). To do this analytically is intractable, but we can get a feel of what happens qualitatively.

As ν decreases from 0, T increases from T_1, meaning c_2 increases and c_1 decreases. This increases the (modulus of the) gradient of the curve f_1 towards $X^\star$. Similarly for f_2, we find that the gradient decreases towards $X^\star$. At $X^\star$, the gradients will be the same (since T is continuous along the line of saddle-node bifurcations) so $X^\star$ is actually a cusp point in the curve of saddle-node bifurcations. This agrees with the data from the AUTO calculations - figure 4 shows cusps points in the curve of saddle-node bifurcations.

We can calculate the locations of the cusp points, since they occur when $\frac{d\nu}{dT} = 0$ along the curve of saddle-node bifurcations. Differentiating equation (22) gives:

$$\frac{d\nu}{dT} = A|\lambda|^2 T\mathrm{e}^{-\lambda_R T}\cos(\lambda_I T + \Phi + \alpha_1(T) + \alpha_2(T)) + O(\mathrm{e}^{-\lambda_R T}, \nu T\mathrm{e}^{-\lambda_R T}) \quad (28)$$

where $\tan(\alpha_2(T)) = \frac{\lambda_I}{-\lambda_R + 1/T}$. So the cusp points occur at

$$\cos(\lambda_I T + \Phi + \alpha_1(T) + \alpha_2(T)) = O\left(\frac{1}{T}, \nu\right) \ll 1$$

so again, since both $\alpha_1(T)$ and $\alpha_2(T)$ are to first order (that is, for large enough T) independent of T, the cusp points will occur with frequency

$$\Delta T = \frac{\pi}{\lambda_I}$$

Let $\cos(\lambda_I T^\star + \Phi + \alpha_1(T^\star)) = -\phi'$, then at $X^\star$, we have (from equation (22)):

$$\nu^\star = A\phi'|\lambda|T^\star\mathrm{e}^{-\lambda_R T^\star} \quad (29)$$

and as expected (25) no longer holds.

The leading order approximating for f at this point gives

$$f^\star = \frac{\nu^\star}{T^\star} + O\left(\frac{\mathrm{e}^{-\lambda_R T}}{T}\right) = A\phi'|\lambda|\mathrm{e}^{-\lambda_R T^\star} + O\left(\frac{\mathrm{e}^{-\lambda_R T}}{T}, \frac{\nu^2}{T}\right) \quad (30)$$

We know the next cusp point occurs at $T \approx T^\star + \frac{\pi}{\lambda_I}$, with $\cos(\lambda_I T + \Phi + \alpha_1(T)) \approx \phi'$. This increase in T is equivalent to rescaling f in (30):

$$f \to -f\mathrm{e}^{-\pi\frac{\lambda_R}{\lambda_I}}$$

5.1 *Comparison with numerical results*

We now compare our analytical findings with data obtained from AUTO calculations for the example from section 2.2. We have already noted the similarities in the structure of the arrangement of the saddle-node bifurcations, shown in figures 7(b) and 4. We use the AUTO data to confirm the re-scalings of f between the cusp points

$$f \to -f\mathrm{e}^{-\pi\frac{\lambda_R}{\lambda_I}}$$

and the difference in the periods of the orbits at the cusp points

$$\Delta T = \frac{\Delta\text{Period}}{6} = \frac{\pi}{\lambda_I}$$

which were obtained from the analytic calculations.

Recall that in our analytic approximations, we assumed the λ_α were constant. In the AUTO calculations, we cannot keep these eigenvalues constant, as the continuation parameters are parameters in the original equations (in this case, e_1 and t). So, as we move towards $f = 0$, not only are the errors in the calculation decreasing (as $T \to \infty$), but also the values of λ_R and λ_I are converging to their values at the codimension-two point.

We show the results from the AUTO calculation in table 2. We give the value of f and T for the periodic orbit at each of the cusp points, and show the ratios/differences between these. Due to the variation in λ_R and λ_I, the convergence is seen more easily if we separate the cusps into two sets, $f > 0$ and $f < 0$. We expect the ratio f_{n-2}/f_n to converge to $\exp(2\pi\frac{\lambda_R}{\lambda_I})$ as $f \to 0$ and the change in the period should converge to $12\pi/\lambda_I$ as $f \to 0$. At the accumulation point (the codimension-two point),

$$\exp^{2\pi\frac{\lambda_R}{\lambda_I}} = 3.98 \qquad \frac{6\pi}{\lambda_I} = \Delta\text{Period} = 22.2$$

These values are close to the limits of the values given in table 2.

There was some difficulty in calculating the value of f at the cusp points from the data provided by AUTO. The continuation parameters (e_1 and t)

Table 2. Showing the values of f at each of the cusp points labelled in figure 4

(n)	f_n	$\left\lvert\frac{f_{n-2}}{f_n}\right\rvert$	Period	ΔPeriod
1	0.057759		66.84	
3	0.022879	2.524	89.45	22.61
5	0.006918	3.307	110.0	20.55
7	0.001805	3.83	131.0	21.0
9	0.00048	3.8	153.0	22.0
(n)	f_n	$\left\lvert\frac{f_{n-2}}{f_n}\right\rvert$	Period	ΔPeriod
2	-0.07118		66.91	
4	-0.014898	4.778	93.99	27.08
6	-0.003576	4.166	118.1	24.11
8	-0.000907	3.93	141.0	22.9
10	-0.0003	3	163.8	22.8

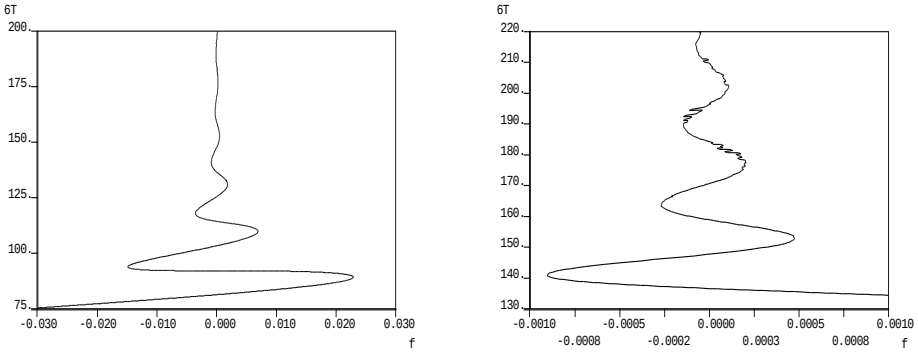

Figure 8. The graph shows the curve of saddle-node bifurcations in the f-T plane, plotted from AUTO output. Parameters are $c_1 = 0.65$, $c_2 = 1.0$, $e_2 = 0.5$, and continuation is in e_1 and t. The right-hand figure is a close up and extension of the top portion of the left-hand figure.

are non-zero at $f = 0$, and the error in f is the same as the error in e_1 and t. Hence, as we approach $f = 0$, since the error in e_1 and t remains constant, the percentage error in f increases. Also we found that for orbits with period $6T \gtrsim 170$, AUTO loses accuracy, as shown in figure 8. Unfortunately, we were unable to improve things by adjusting the discretisation and computation constants in AUTO.

The values of f in table 2 correspond to the maxima and minima of f along the curve of saddle-node bifurcations, from the data shown in figure 8. The values were calculated by fitting a least squares quadratic to 5 or 7 points around each maxima. This was repeated for two different data sets (with different step size in AUTO) and the number of significant figures shown in

the table is that to which the two methods agreed.

6 Conclusions

In this paper we have studied a robust heteroclinic cycle in $\mathbb{R}^6$ which has a pair of complex conjugate radial eigenvalues at each equilibrium. The robustness arises because the vector field commutes with an action of $\mathbb{Z}_6 \ltimes (\mathbb{Z}_2)^6$.

We first considered the codimension-one resonant bifurcation of the cycle and showed that it is associated with the birth or death of a nearby (long period) periodic orbit. This periodic orbit undergoes a further series of saddle-node bifurcations. The bifurcation can occur subcritically or supercritically. We introduce a second bifurcation parameter to unfold the degeneracy which occurs when the bifurcation is neither subcritical nor supercritical.

We then found that there is a repeating structure of saddle-node bifurcations about the codimension-two point, with a well-defined scaling as we approach the codimension-two point. The analytical findings were compared with numerical results and good agreement was found.

We expect that similar results may be found for bifurcations of similar heteroclinic cycles in systems commuting with symmetry groups $\mathbb{Z}_n \ltimes (\mathbb{Z}_2)^n$, $n \geq 5$, although we have not yet looked at any specific examples. These groups are important in an ecological context; many examples of ODEs describing population models commute with a group of this form, see Hofbauer [3].

Much of the structure in our problem arises as a result of the complex eigenvalues at the equilibria in the cycle. We expect that if the complex eigenvalues were not present, the situation would be simpler. The codimension-two bifurcation in the real eigenvalue case would have a structure similar to that shown in figure 9. The curve of saddle-node bifurcations predicted for this case (the dashed line in figure 9(a)) is monotonic, rather than spiralling through a sequence of cusps. This predicted bifurcation diagram is very similar to that found in the resonant homoclinic bifurcation [12] in the non-robust case.

It is expected that such a bifurcation diagram would be found near the codimension-two point for a resonant bifurcation in the real eigenvalue case. To the best of the authors knowledge this has not been demonstrated however; both the Guckenheimer–Holmes cycles and the example of Field and Swift [14] are degenerate at the codimension-two point when only linear and cubic terms are included. In either case, we may be able to break the degeneracies by adding appropriate fifth order terms to these vector fields.

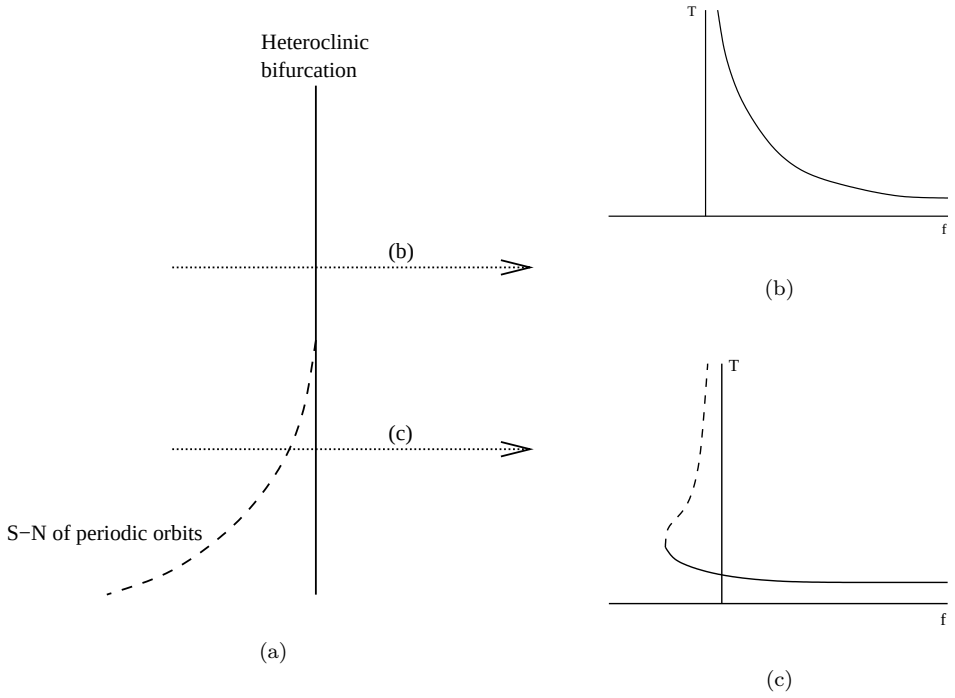

Figure 9. (a) shows a conjectured bifurcation diagram of a codimension-two resonant bifurcation from a heteroclinic cycle with real eigenvalues. (b) and (c) show the periods and locations of the bifurcating periodic orbits for two sections across the diagram, as indicated.

Acknowledgements

The authors would like to thank Mike Field for helpful discussions. CMP is funded by the EPSRC. JHPD is supported by Trinity College, Cambridge and Newnham College, Cambridge.

Appendix A: Eigenvalue data

In the appendix we set out explicit expressions for the eigenvalues λ_α at the equilibria for the ODEs on the cycle. First, let

$$D = 2e_1c_1 + c_1^2 + c_2e_2 + 2c_2c_1 + c_2c_1^2 + 2e_2e_1 + e_1^2 - e_2e_1^2$$

Then

$$\lambda_R = (c_2c_1^2 - e_2e_1^2)/D$$

$$\begin{aligned}\lambda_I = (&3c_2^2c_1^4 + 18c_2c_1^2e_2e_1^2 + 3e_2^2e_1^4 + 8c_2^2c_1^2e_2e_1 + 8e_1^3c_2e_2c_1 + 4e_1^3c_2c_1^2 \\ &+ 8e_1^2c_2c_1^3 + 8e_1^3c_1^2e_2 + 4c_2^2c_1^3e_1 + 4e_1^4e_2c_1 + 8e_1c_1^3c_2e_2 + 8e_1^2c_1c_2e_2^2 \\ &+ 4e_1^2c_1^3e_2 + 4e_1c_1^4c_2 + 4c_1^3c_2^2e_2 + 4e_1^3c_1e_2^2 + 4e_2^2e_1^3c_2 + 4e_1c_1c_2^2e_2^2)^{1/2}/D\end{aligned}$$

$$\lambda_t = (-c_2c_1^2 + e_2e_1^2 - e_2^2e_1 + tc_2e_2 + c_2^2c_1 + c_2e_1^2 - c_1e_2e_1 + tc_2c_1 + te_2e_1 + c_2c_1e_1 - c_1^2e_2)/D$$

$$\lambda_c = (-c_2c_1^2 + e_2e_1^2 + c_1e_2e_1 - c_2e_2^2 + tc_2c_1 + te_1^2 + c_1^2e_1 - c_2c_1e_2 - e_2^2e_1 + tc_1e_1 + c_1^3)/D$$

$$\lambda_e = (c_2c_1^2 - e_2e_1^2 - te_2e_1 - c_2^2e_2 + c_2c_1e_1 + e_1^3 - tc_1e_1 - c_2^2c_1 - c_2e_2e_1 + c_1e_1^2 - tc_1^2)/D$$

For the heteroclinic cycle to exist as we describe we require $\lambda_R, \lambda_t, \lambda_c, \lambda_e > 0$.

References

[1] Golubitsky, M., Stewart, I. N. and Schaeffer, D.G., 1998, *Singularities and Groups in Bifurcation Theory. Volume II.* Springer, Applied Mathematical Sciences Series **69**.

[2] Golubitsky, M. and Stewart, I., 2002, The symmetry perspective. Progress in Mathematics, volume 200, Birkäuser.

[3] Hofbauer, J. and Sigmund, K., 1998, *Evolutionary Games and Population Dynamics*, CUP.

[4] Krupa, M., 1997, Robust heteroclinic cycles. *J. Nonlinear Sci.*, **7** 129-176.

[5] Guckenheimer, J. and Holmes, P., 1988, Structurally stable heteroclinic cycles. *Math. Proc. Camb. Phil. Soc.*, **103** 189-192.

[6] Busse, F. H. and Heikes, K. E., 1980, Convection in a rotating layer: A simple case of turbulence. *Science*, **208**, 173-175.

[7] May, R. M. and Leonard, W., 1975, Nonlinear aspects of competition between three species. *SIAM J. Appl. Math.*, **29**, 243-253.

[8] Krupa, M. and Melbourne, I., 1995, Asymptotic stability of heteroclinic cycles in systems with symmetry. *Ergod. Th. & Dynam. Sys.*, **15** 121-147.

[9] Chossat, P., Krupa, M., Melbourne, I. and Scheel, A., 1997, Transverse bifurcations of homoclinic cycles. *Physica D*, **100**, 85-100.

[10] Krupa, M. and Melbourne, I., 2004, Asymptotic stability of heteroclinic cycles in systems with symmetry, II. *Proc. Roy. Soc. Edinburgh A*, **134A**, 1177-1197.

[11] Postlethwaite, C. M., 2005, Stability results for a class of robust homoclinic cycles in $\mathbb{R}^n$. *In preparation.*

[12] Chow, S.-N., Deng, B. and Fielder, B., 1990, Homoclinic bifurcation at resonant eigenvalues, *J. Dyn. Diff. Eq.* **2**, 177-244.

[13] Homburg, A. J. and Krauskopf, B., 2000, Resonant Homoclinic Flip Bifurcations, *J. Dyn. Diff. Eq.* **12**, 807-850.

[14] Field, M. J. and Swift, J., 1991, Stationary bifurcation to limit cycles and heteroclinic cycles. *Nonlinearity*, **4**, 1001-1043.

[15] Hofbauer, J., 1994 Heteroclinic Cycles in Ecological Differential Equations *Tatra Mountains Math. Publ.* **4** 105-116

[16] Postlethwaite, C. M. and Dawes, J. H. P., 2005, Regular and irregular cycling near a heteroclinic network *Nonlinearity*, **18**, 1477-1509.

[17] Field, M. J., 1996, *Lectures on bifurcations, dynamics and symmetry.* Pitman Research Notes in Mathematics, vol. 356. London: Longman Scientific and Technical.

[18] Doedel, E., Champneys, A., Fairgrieve, T., Kuznetsov, Y., Sandstede, B. and Wang X., 1997, *AUTO97: Continuation and bifurcation software for ordinary differential equations.* Available via FTP from directory `pub/doedel/auto` at `ftp.cs.concordia.ca`.